Geophys. J. Int. (2006) **167,** 213–222 doi: 10.1111/j.1365-246X.2006.03042.x

The crustal structure of the eastern Marmara region, Turkey by teleseismic receiver functions

Ekrem Zor,[1,*] Serdar Özalaybey[2] and Cemil Gürbüz[3]

[1]*Department of Geological Sciences, University of Missouri-Columbia, MO 65211-1380, USA. E-mail: zore@missouri.edu*
[2]*Earth and Marine Sciences Institute, TÜBİTAK, Marmara Research Center, Gebze-Kocaeli, Turkey*
[3]*Department of Geophysics, Kandilli Observatory and ERI, Boğaziçi University, Çengelköy-İstanbul, Turkey*

Accepted 2006 April 20. Received 2006 April 12; in original form 2005 April 25

SUMMARY

We study the crustal structure of eastern Marmara region by applying the receiver function method to the data obtained from the 11 broad-band stations that have been in operation since the 1999 İzmit earthquake. The stacked single-event receiver functions were modelled by an inversion algorithm based on a five-layered crustal velocity model to reveal the first-order shear-velocity discontinuities with a minimum degree of trade-off. We observe crustal thickening from west (29–32 km) to east (34–35 km) along the North Anatolian Fault Zone (NAFZ), but we observe no obvious crustal thickness variation from north to south while crossing the NAFZ. The crust is thinnest beneath station TER (29 km), located near the Black Sea coast in the west and thickest beneath station TAR (35 km), located inland in the southeast. The average crustal thickness and *S*-wave velocity for the whole regions are 31 ± 2 km and 3.64 ± 0.15 km s^{-1}, respectively. The eastern Marmara region with its average crustal thickness, high heat flow value (101 ± 11 mW m^{-2}) and with its remarkable extensional features seems to have a Basin and Range type characteristics, but the higher average shear velocities ($\sim$3.64 km s^{-1}) and crustal thickening from 29 to 35 km towards the easternmost stations indicate that the crustal structure shows a transitional tectonic regime. Therefore, we conclude that the eastern Marmara region seems to be a transition zone between the Marmara Sea extensional domain and the continental Anatolian inland region.

Key words: crustal structure, eastern Marmara region, inversion, receiver function.

1 INTRODUCTION

The crustal structure of the eastern Marmara region of Turkey has been investigated by using broad-band data available from the two modern seismic networks that have been in operation since the 1999 İzmit earthquake. This earthquake devastated most of the Marmara region where the North Anatolian Fault Zone (NAFZ), a well-known continental strike-slip fault, has recently been mapped to run across the Sea of Marmara (Le Pichon *et al.* 2001) and where very limited geophysical experiments exist to evaluate the crustal structure across the NAFZ. In this paper, we apply the receiver function method to the broad-band data and present crustal shear wave velocity models for 11 stations installed within three different tectonic zones separated by the NAFZ to infer variations in the crustal structure. The receiver function method has recently been successfully used in the eastern Turkey to evaluate the variations in the crustal structure and address some key questions concerning the tectonic evolution of this region (Zor *et al.* 2003). Receiver function inversions for shear wave velocity structure from teleseismic body waves have been used to constrain the depth of any large velocity discontinuities in the areas of interest around the world for the last two decades (Langston 1979a; Ammon *et al.* 1993; Özalaybey *et al.* 1997; Kind *et al.* 2002, so on). The receiver functions, which are sensitive to changes in shear wave velocity, are extracted from three-component broad-band recordings of teleseismic waveforms, using a deconvolution process that is aimed to enhance *P*-to-*S* converted waves generated near the recording station (Langston 1979). Besides the difficulties and costs to obtain crustal structure using wide angle refraction and reflection experiments, the inversions of receiver functions are a simple, reliable and cost-effective way of obtaining shear velocity structure beneath a broad-band station.

2 GEOLOGY

After the closing of the Neo–Tethys, the African–Arabian plate collided and subducted beneath the Anatolia and Aegean continents (Şengör & Yılmaz 1981). The collision causes westward movement of the Anatolian microplate between two prominent strike-slip fault zones (Rotstein & Kafka 1982). These fault zones are the left lateral East Anatolian Fault Zone (EAFZ) in eastern Turkey and right

*Now at: Earth and Marine Sciences Institute, TÜBİTAK, Marmara Research Center, Gebze-Kocaeli, Turkey.

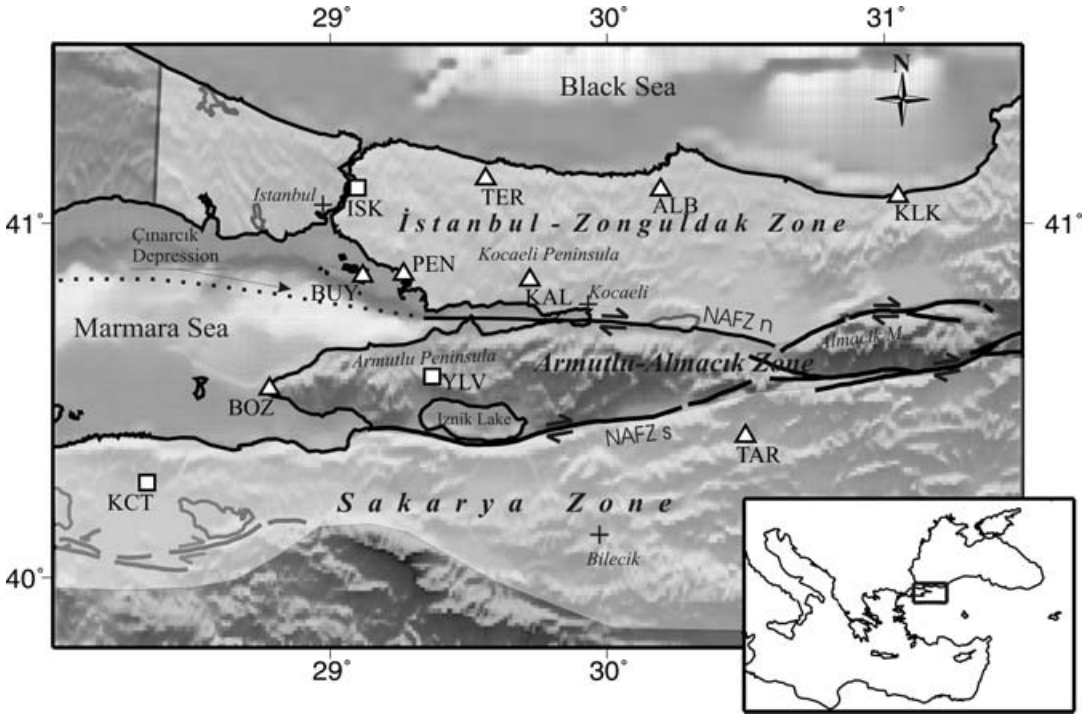

Figure 1. Locations of the stations used in the analysis plotted on the grey-shaded topography and bathymetry. The eight stations with broad-band seismographs operated by the MRC are symbolized with triangles and the three broad-band stations of KOERI with squares. The solid lines show the trace of the NAFZ. The plus signs show city locations. The dotted line shows the probable continuation of the NAFZ under the Marmara Sea. The Armutlu–Almacık Zone is bounded by northern, NAFZn, and southern, NAFZs, branches of the NAFZ and situated between the İstanbul–Zonguldak and Sakarya Zones which are shaded white on the map.

lateral NAFZ. The NAFZ is a well-recognized continental strike-slip fault zone in the world because of its remarkable seismic activity and extremely well-developed surface expression (Fig. 1). Several depressions such as Çınarcik Depression in the Marmara Sea are aligned along the NAFZ. The NAFZ was initiated in the eastern Anatolia during Late Miocene and propagated westwards reaching the Marmara Sea region during Pliocene (Şengör 1979; Barka 1992; Görür *et al.* 1997; Okay *et al.* 1999; Tüysüz *et al.* 1998).

The eastern Marmara region can be divided into three zones as in Fig. 1, taking into consideration pre- and post-early Cretaceous event and tectonic entity formed Northern zone, Intermediate zone and Southern zone (Yılmaz *et al.* 1997). The Northern zone covers an area consisting of İstanbul–Zonguldak tectonic unit and its Cretaceous–Tertiary cover succession which crops out in the Kocaeli Peninsula. The Southern zone is represented by basement metamorphic rocks of Sakarya Zone and its cover succession. The Southern zone crops out around Bilecik. The Intermediate zone extends between these distinctly different two zones in and around Armutlu Peninsula and Almacık Mountain. This zone has a complex basement composed of fragments of both İstanbul–Zonguldak tectonic unit and the Sakarya Zone. The northern and southern branches of the NAFZ run along the northern and southern edge of the Armutlu Peninsula, respectively (Fig. 1).

3 PREVIOUS GEOPHYSICAL STUDIES

For the last four decades, several seismological studies have been carried out around the Marmara region to investigate its crustal structure by using passive sources (earthquake) (Canıtez 1962; Crampin & Üçer 1975; Kenar 1978; Necioğlu *et al.* 1981; Karabulut *et al.* 2002; Özalaybey *et al.* 2002) and active sources data (seismic explosions and quarry blasts) (Gürbüz *et al.* 1979; Gürbüz & Üçer 1980; Karahan *et al.* 2001; Karabulut *et al.* 2003).

These crustal studies aimed to resolve crustal thickness variation as well as crustal velocity function mostly to improve earthquake epicentres and depths accurately in the region. Most of them reported their crustal thickness estimates, but they do not correlate their results with geologic structure in detail. Canıtez (1962) found the crustal thickness as 31 km using passive source data and it may be thinner in the north than in the south based on active source data along the seismic profiles crossing the NAFZ. The thinner crustal estimate is 25 km around İstanbul from the quarry blast study by Gürbüz & Üçer (1980) and Kenar (1978) also found that the crustal thickness in the same area is between 25 and 30 km, using *P*-wave amplitude spectrums of earthquake recordings. Necioğlu *et al.* (1981) found 28-km-thick crust using earthquakes recorded around the Marmara region. Özalaybey *et al.* (2002) and Karabulut *et al.* (2002) also derived velocity models using different data set from the aftershocks following the 1999 August 17 Kocaeli earthquake ($M_w = 7.4$) and found average 33-km crust for the eastern Marmara region. A recent study around the eastern Marmara region found the thicker crustal estimate as 39 km using controlled source data by Karahan *et al.* (2001). Using all these studies, the reported *P*-wave velocities averaged over the crust and uppermost mantle in the region are between 5.7 and 6.4 km s^{-1} and 8.0 and 8.1 km s^{-1}, respectively.

4 DATA

We process teleseismic waveforms recorded by eight broad-band stations (BOZ, BUY, PEN, KAL, TAR, TER, ALB and KLK)

Table 1. The teleseismic earthquakes used in the receiver function analysis (ISC).

	Otime (yr jd hr:min)	Depth	M	Δ	BAZ	KAL	TER	ALB	KLK	ISK	BUY	PEN	BOZ	YLV	KCT	TAR
1	1998 232 15:00	33	6.2	83	20					×						
2	1998 235 05:36	70	6.7	81	78					×						
3	1998 323 15:39	10	6.0	80	69					×						
4	1999 024 00:37	33	6.3	79	59					×						
5	1999 028 08:10	67	6.3	67	85					×						
6	1999 067 12:25	33	6.5	78	29					×						
7	1999 098 13:10	560	6.4	70	49					×				×	×	
8	1999 132 17:59	98	6.3	78	43					×						
9	1999 263 17:57	33	6.5	76	70			×	×					×	×	×
10	1999 265 00:14	26	6.2	76	71									×		
11	1999 268 23:52	17	6.2	76	70			×	×	×						×
12	1999 305 17:53	33	6.1	77	71					×						×
13	1999 319 05:42	10	6.3	68	112	×	×	×	×			×				×
14	1999 340 23:22	50	6.0	82	3								×			×
15	1999 341 00:19	41	6.5	82	3			×			×					×
16	1999 345 18:03	33	6.5	80	78	×	×		×		×		×			
17	1999 355 14:14	56	6.2	85	104		×		×				×			
18	2000 006 21:31	33	6.1	80	167						×		×			×
19	2000 028 14:21	61	6.7	80	41		×	×		×			×			×
20	2000 088 11:00	127	6.8	92	58			×		×	×			×		×
21	2000 156 16:28	33	6.8	81	105	×			×				×			
22	2000 158 14:57	33	6.0	80	60			×	×	×			×			
23	2000 158 21:16	10	6.0	79	52			×		×			×			
24	2000 159 23:45	33	6.1	80	105	×		×	×			×	×			
25	2000 161 08:00	33	6.0	82	105								×			
26	2000 162 18:23	33	6.2	77	70			×	×	×			×			×
27	2000 170 14:44	10	7.1	83	114	×		×				×	×			×
28	2000 177 06:34	10	6.3*	79	59								×			
29	2000 190 04:52	33	6.0*	81	105								×			
30	2000 190 18:57	10	6.2	82	52								×			
31	2000 193 01:32	56	6.5	82	2	×		×					×			
32	2000 198 03:21	33	6.2	79	72	×	×						×			
33	2000 212 12:25	10	6.3	82	52								×			
34	2000 217 21:13	10	7.0	73	39	×	×	×					×			
35	2000 219 07:27	452	6.7	86	55	×	×						×			
36	2001 010 16:02	33	6.2	83	1	×					×		×			×
37	2001 044 19:28	33	6.5	81	105	×	×						×			×
38	2001 055 07:23	33	6.6	94	84							×				
39	2001 059 18:54	49	5.9	89	342	×										×
40	2001 083 06:27	33	5.9	77	56	×	×						×			×
41	2001 104 23:27	33	6.1	86	53							×	×			

installed by the Marmara Research Center (MRC) of Scientific and Technical Research Council of Turkey, following the 1999 August 17 Kocaeli earthquake ($M_w = 7.4$) and three permanent broad-band stations (KCT, YLV and ISK) operated by the Bogazici University, Kandilli Observatory and Earthquake Research Institute (KOERI) around the Marmara region (Fig. 1). The MRC seismological network was mainly installed for monitoring the aftershock seismicity of the 1999 Izmit earthquake ($M_w = 7.4$). The eight MRC stations are equipped with Guralp broad-band three-component sensors (CMG-40T) and three-channel 24-bit Reftek digital recorders with GPS timing. These stations are capable of recording seismic signals with a flat velocity response in the frequency range 0.03–50 Hz. The three KOERI stations are the permanent stations in which KCT and YLV were equipped with Guralp broad-band three-component sensors having the same velocity response as the MRC stations, while station ISK has a Guralp broad-band sensor having a flat velocity response in the frequency range 0.01–50 Hz. All stations record seismic signals in continuous mode using a 100 sps sampling rate. Approximately, 150 teleseismic events were extracted from the continuous broad-band recordings ranging from 35 to 95 epicentral distances with a magnitude greater than 5.8. Because of data loss (technical difficulties such as power, telemetric communication problems) and low signal-to-noise ratio (S/N), the remaining 41 teleseismic events listed in Table 1 have been used in the receiver function analysis (Fig. 2).

5 METHOD

We invert *P*-wave receiver functions by using a grid search modelling technique (Sandvol *et al.* 1998; Zor *et al.* 2003). Langston (1979a) proposed a technique to obtain a time-series dominated by a local structure effect (receiver function) by deconvolving the vertical component from the horizontal components of motion. We use the iterative time-domain deconvolution method proposed by Liggoria & Ammon (1999) to obtain receiver functions, because this method is more stable for the low frequencies and perform well under low-S/N conditions. Since we are primarily interested in determining the

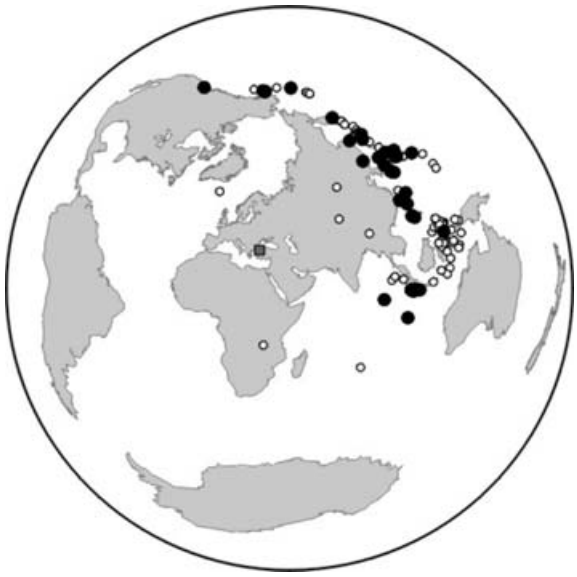

Figure 2. The black dots show the locations of teleseismic events used in the receiver function analysis and the black circles show all the events between the dates in Table 1; they are ranging from 35 to 95 epicentral distances and their magnitudes are greater than 5.8.

first-order variations in the crustal velocity discontinuities and their depths, hence we are willing to lose resolution of crustal structure in order to minimize the effects of small-scale 'non-one-dimensional' structures beneath the receivers. Thus, we use a Gaussian filter with a width of 1.5 (∼1 Hz) in the extraction process of receiver functions from the raw broad-band seismograms. Such a choice of Gaussian filter helps to reduce the effects of unwanted scattered energy at the cost of resolution of the crustal structure.

We model the stacked radial *P*-wave receiver functions for each station by using a grid search inversion scheme assuming homogeneous, isotropic and plane layered crustal structure. Our grid search inversion uses a five-plane layered structure instead of using an inversion scheme that uses many-plane layered structures. Such inversion schemes suffer from high evaluation cost and the non-uniqueness problem inherent in the receiver functions when no *a priori* and/or additional geophysical constraints included in the receiver function inversion. Average crustal *P*-wave velocities in the region obtained from previous studies indicate a rather large range (5.7–6.4 km s^{-1}) and surface wave dispersion measurements are not yet available in our study region. The joint inversion of receiver functions and dispersion data, which is invaluable for obtaining a well-constrained velocity structure as shown by Özalaybey *et al.* (1997), is not suitable for our current data set since reliable dispersion data do not exist yet. Thus, we aim to find the first-order discontinuities revealed by the first-order features that are present in our observed receiver functions. A grid search scheme seems to be a more suitable method for our data set since we parametrize the unknown model space using a small number of model parameters, five-plane layered structure with unknown shear velocities and thicknesses and, thus, we are able to employ a complete grid search throughout the whole unknown model parameters while avoiding the use of too many free model parameters and any initial models. We apply the grid search inversion scheme using a grid spacing of 0.2 km s^{-1} for the shear wave velocity and 2 km for layer thicknesses for each layer. We specify upper and lower bounds for shear velocity and thickness in each layer. Table 2 gives the summary information on the grid search parametrization for each layer.

Table 2. Parameter space used in the grid search inversion method.

Layer	$\Delta\beta$	Δth	Min β	Max β	Min th	Max th
1	0.20	2.0	1.40	3.60	2.0	6.0
2	0.20	2.0	3.00	4.00	6.0	16.0
3	0.20	2.0	3.00	4.40	6.0	16.0
4	0.20	2.0	3.00	4.40	6.0	16.0
5	0.10	2.0	4.40	4.80	5.0	5.0

The grid search methodology is based on examining the fitness function to find the velocity model, which gives the largest fitness value between the observed and modelled synthetic receiver functions. We define our fitness function as the semblance value (Neidell & Taner 1971) between the observed and synthetic receiver functions. A technique based on propagator matrix method developed by Kennett (1983) is used to generate synthetic receiver functions as a forward modelling operator. We calculate the fitness function for all model parameters and keep the entire values of the fitness function for each velocity model and the associated synthetic receiver function (Zor *et al.* 2003). Then, we select a group of velocity models from the entire space of sampled fitness function based on a threshold value. This threshold value is usually 2 per cent lower than apparent best fit in terms of semblance values. Such selection process results in a reduced number of acceptable velocity models that can fit the observed receiver functions. Further elimination of the selected velocity models is achieved by employing average crustal velocity constraints obtained from the previous studies. After *a priori* constraints for average crustal velocity are applied, the number of velocity models which fit observed data is reduced mostly to one and sometimes two alternatives from which one was picked as the optimum velocity model for each station. In order to place uncertainty bounds on the selected optimum velocity models, we employ a sensitivity analysis by thoroughly exploring the model space through forward modelling as described by Özalaybey *et al.* (1997).

6 RECEIVER FUNCTIONS

Since deep events with simple pulse-like waveforms on the vertical component are preferred to use in the receiver function analysis, the location of the study area and its proximity with respect to subduction, collision sites play an important role in obtaining a good azimuthal coverage. Stations in the eastern Marmara region effectively record the teleseismic events mostly coming from the northeast (between 0 and 120 backazimuths). In this study, 114 high-quality broad-band recordings of 41 teleseismic events ranging from 67° to 94° epicentral distances with a magnitude greater than 5.9 were chosen for the receiver function inversion. Since the number of closer events was not enough to make a separate stack, they were not inverted. Fig. 2 shows the distribution of the events and Table 1 lists the teleseismic event parameters that are used in the receiver function analysis. In order to decrease uncorrelated noise and signal generated scattered energy (e.g. scattered energy from non-one-dimensional structures), the single-event receiver functions were stacked by grouping them according to backazimuth. In the absence of the events other than mostly the northeast (NE) as stated before and southeast (SE) quadrants (Fig. 2), we stacked all receiver functions obtained from the selected waveforms.

In order to see the coherency between the observed receiver functions and the tectonic zones they belong to, we group the stations as northern, intermediate, and southern stations. The northern

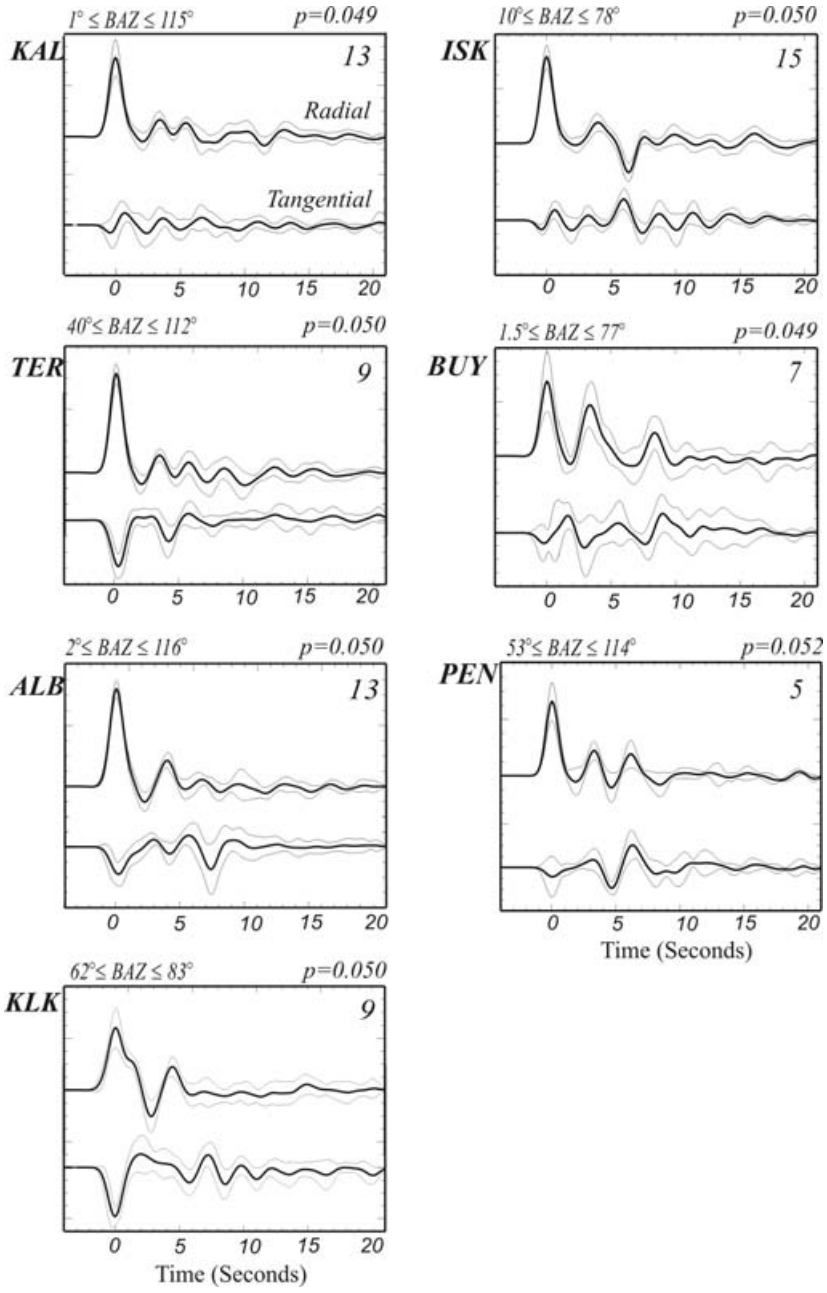

Figure 3. Stacked radial and tangential receiver functions for the northern stations; the bold lines show mean receiver functions and the grey lines show their standard deviation bounds obtained from the stacking process. The numbers in the upper right-hand corner show the number of receiver functions that were used to stack. Backazimuth range and average slowness values are also indicated.

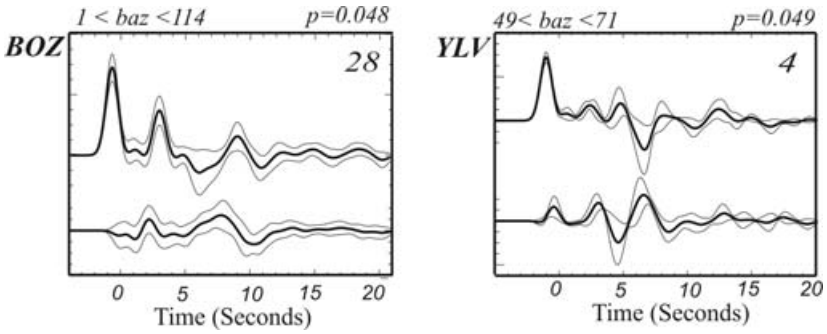

Figure 4. Stacked receiver functions for the intermediate stations, the figure format is the same as Fig. 3.

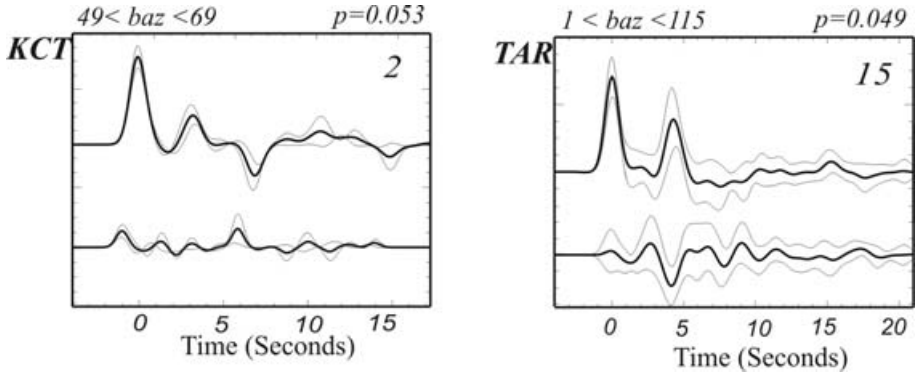

Figure 5. Stacked receiver functions for the southern stations, the figure format is the same as Fig. 3.

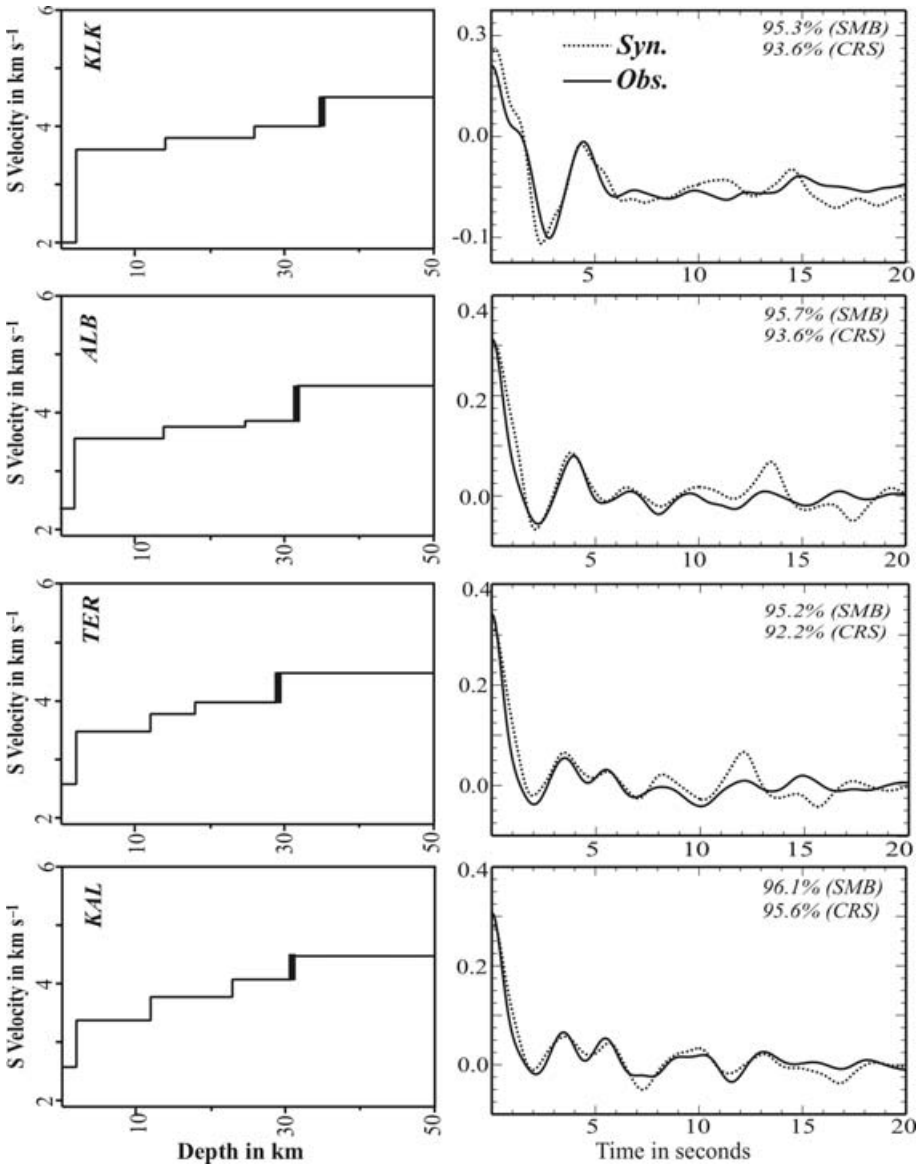

Figure 6. Velocity–depth functions obtained for the northern stations. The waveform fits obtained from the inversion are shown in the lower panel. The bold and dashed lines show observed and modelled synthetic receiver functions, respectively. The numbers on the waveform fits show semblance (SMB) and cross-correlation (CRS) fitness values.

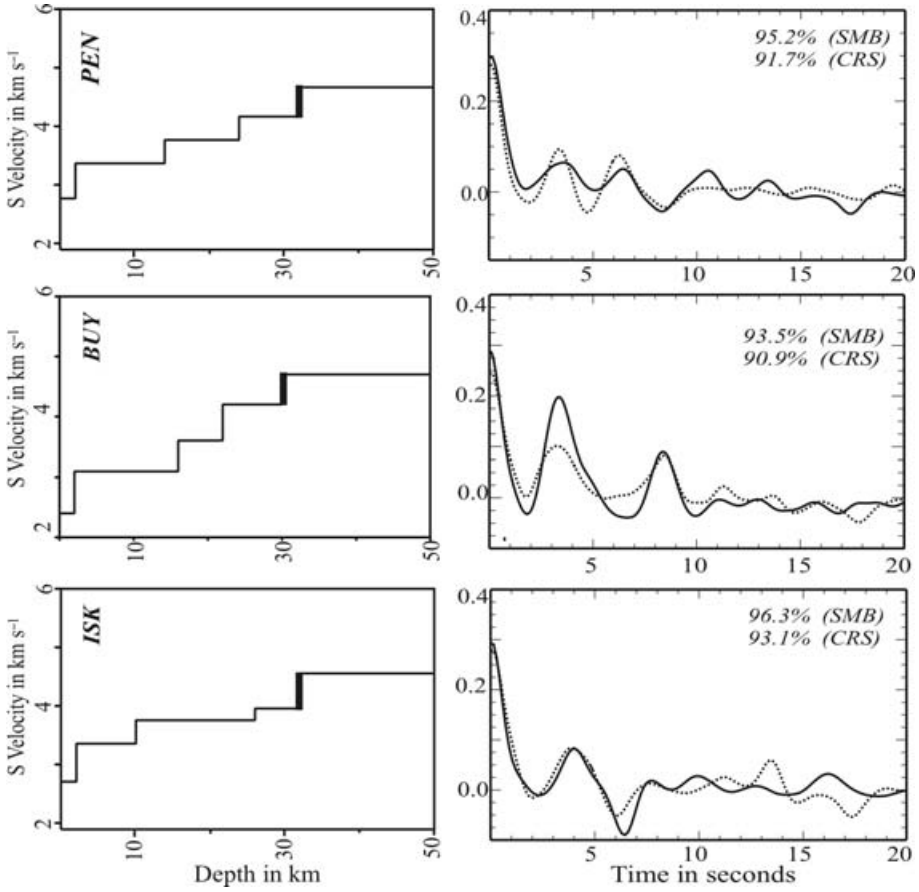

Figure 6. (*Continued.*)

stations ISK, BUY, PEN, KAL, TER, ALB and KLK are installed on the İstanbul–Zonguldak Zone. Among these stations, BUY is situated on an island, which is very close to the Çınarcık depression (Fig. 1). The intermediate stations BOZ and YLV are installed on the Armutlu–Almacık Zone and the southern stations KCT and TAR are located on the Sakarya Zone (Fig. 1). The receiver functions of the northern stations are stacked and standard deviation bounds for each station are shown in Fig. 3. As can be seen from the figure, the radial receiver functions for KAL and TER have remarkably similar converted arrivals for the first 8 s. Later arrivals observed on the radial receiver functions of KAL and TER do not show such similarity. Another considerable feature on the northern stations, their tangential receiver functions show a similar first negative swing of motion. The station TER has a remarkable negative first swing, which is also similarly observed on the other northern stations ALB and KLK, not displayed as strongly as on station KAL. This variation on the tangential receiver function may suggest a dipping structure. On the other hand, we observe no great similarity between the receiver functions of stations PEN and BUY, although they are on the same tectonic unit and are geographically very close. This may be the result of suspected scattered energy that is present in the BUY receiver functions since this station is located in an island of the Marmara Sea at the proximity of the Çınarcık depression that might cause scattering and distortion on the observed receiver functions compared to the PEN receiver functions that are obtained from an inland station. Such suspected scattered energy may be evident from the large standard deviation bounds on the stacked radial as well as tangential receiver functions of station BUY (Fig. 3). For the intermediate stations in Fig. 4, station YLV did not provide as many useful receiver functions as station BOZ since this station had operational difficulties and thus did not provide as much data. We only obtain four good-quality receiver functions for station YLV. Similarly, a southern station KCT has only two receiver functions to be stacked (Fig. 5). Thus, receiver functions for these stations have relatively lower S/N. To obtain quantitative images about the crustal structure, we apply the grid search inversion of the observed receiver functions described in the previous section (Sandvol *et al.* 1998; Zor *et al.* 2003).

7 INVERSION RESULTS

We present optimum velocity models and their waveform fits as northern, intermediate and southern stations in this section. The estimated velocity models for the northern stations ISK, PEN, TER, KAL, ALB and KLK are quite similar with some small differences in the velocities and thicknesses of individual layers and they are shown along with their waveform fits in Fig. 6. We do not observe similarity between the estimated velocity models of stations BUY and PEN as they have quite different receiver functions discussed in the previous section. On the other hand, the derived velocity model of station KAL is slightly different from that of station TER. The inversion results for the northern stations also show that the velocity of the sedimentary layer decreases towards the east from 2.8 to 2.1 km s^{-1} and also high velocity contrast between the sedimentary layer and the second layer is observed as the velocities jump from an average value of 2.5 to 3.5 km s^{-1}. This layer extends down to

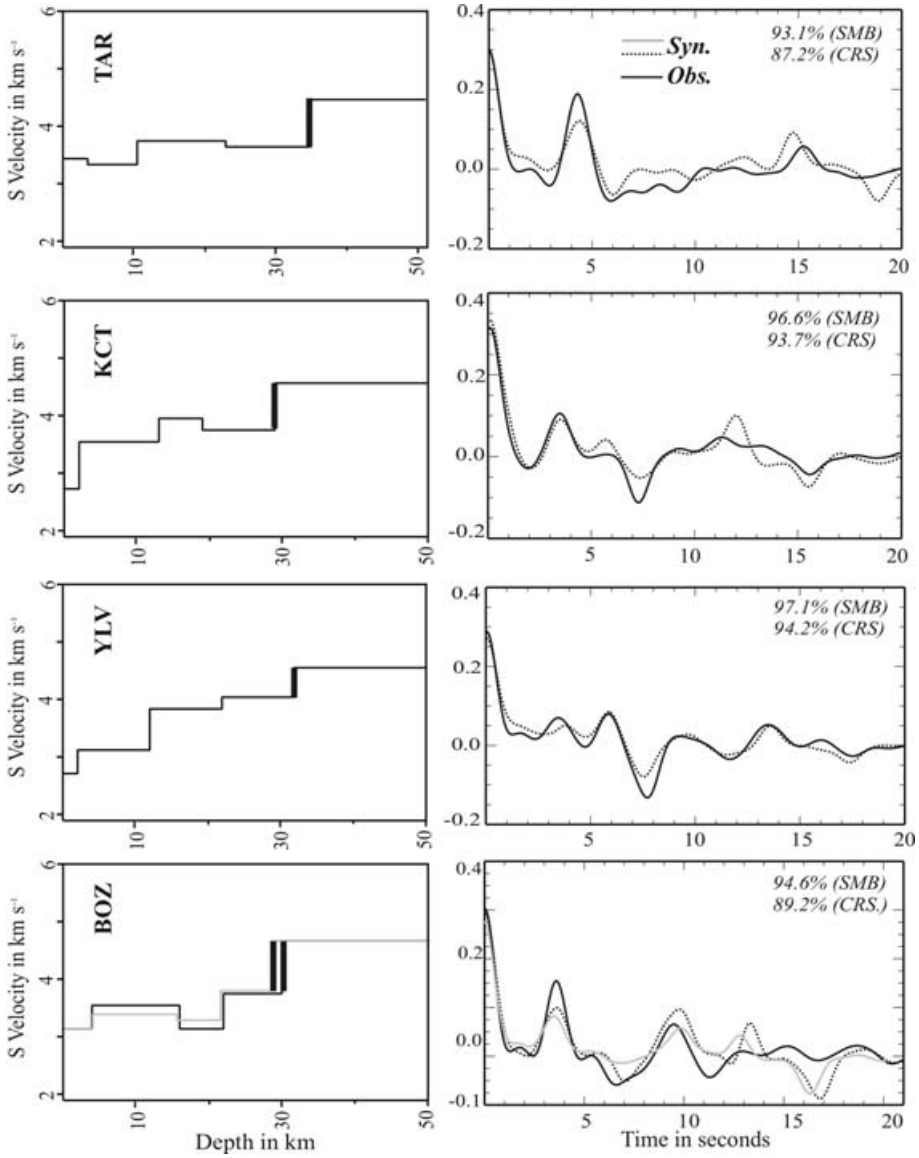

Figure 7. The intermediate (two on the right-hand panel) and southern (two on the left-hand panel) station waveform fits and the estimated velocity models.

10–15 km depths. Third layer of station TER is thinner than the other stations and the Moho depth increases towards the east from 29 to 34 km. The crustal thicknesses for northern stations ISK, BUY, PEN, TER, KAL, ALB and KLK are determined to be 32, 30, 30, 29, 31, 32 and 34 km, respectively (Fig. 6).

The estimated velocity models for the intermediate stations, BOZ and YLV, have no similarities with each other. It is interesting to observe that KAL and YLV velocity functions are almost identical to each other (Fig. 6 and 7). A small difference between YLV and KAL velocity models is that station YLV velocity model does not jump as strong as the northern station velocity models from the first layer to the second layer (2.8 to 3.2 km s^{-1}), but it has a strong contrast from the second layer to the third layer (3.2 to 3.9 km s^{-1}) around 10 km and after that the velocity gradually increases down to the Moho depth. Station BOZ does show the possibility of a low-velocity zone (LVZ) located around 20 km and we could not model the negative phases around 6 s for the mean receiver function without having an LVZ as seen in Fig. 7. For a given standard deviation bound around 6 s for this station (Fig. 4), it is also possible to have velocity models with no LVZ. The receiver function for this velocity model fits the other part of the observed receiver function except the negative phase around 6 s. The crustal thicknesses derived from the estimated velocity models for stations YLV and BOZ are 30 and 32 km, respectively (Fig. 7).

In the southern part, the stations KCT and TAR are far from each other, but both lie on the Sakarya Zone. The velocity of the first layer for station KCT (2.8 km s^{-1}) is lower than that of station TAR (∼3.4 km s^{-1}). TAR velocity model shows a simple two-layered structure, which extends down to 10 km depth with a velocity of 3.4 km s^{-1} and jumps to 3.8 km s^{-1} extending to the Moho depth. There is a remarkable difference in the crustal thickness from 29 km at station KCT to 35 km at station TAR. The optimum shear wave velocity models found for each station along with their crustal thicknesses, average crustal and upper mantle velocities are summarized in Table 3.

In order to establish error bounds on the estimated crustal parameters, we apply a sensitivity analysis on the optimum shear wave velocity models (Özalaybey *et al.* 1997). Each layer velocity and

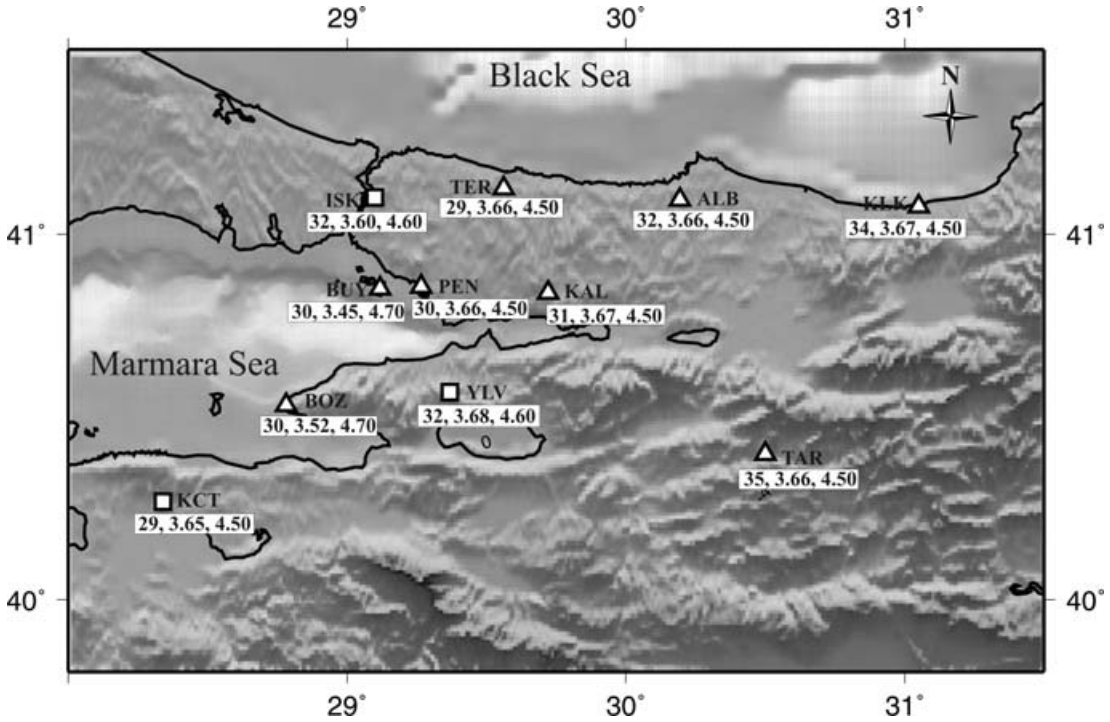

Figure 8. Grey-shaded bathymetry–topography map of the eastern Marmara region plotted with crustal thickness (km), mean crustal shear wave velocity (km s^{-1}) and upper mantle shear velocity (km s^{-1}), respectively, shown under each station.

Table 3. Five-layered velocity model for each station. The rightmost column shows crustal velocity and thickness.

Stations		Layers					Crustal velocity V_s and thickness
		1	2	3	4	5	
ISK	V_s	2.75	3.40	3.70	3.90	4.60	3.60
	h	2.00	8.00	16.00	6.00		32.00
TER	V_s	2.60	3.50	3.75	3.95	4.50	3.66
	h	2.00	10.00	6.00	11.00		29.00
ALB	V_s	2.40	3.60	3.80	3.90	4.50	3.66
	h	2.00	12.00	11.00	7.00		32.00
KLK	V_s	2.00	3.60	3.80	4.00	4.50	3.67
	h	2.00	12.00	12.00	8.00		34.00
BUY	V_s	2.40	3.10	3.60	4.20	4.70	3.45
	h	2.00	14.00	6.00	8.00		30.00
KAL	V_s	2.60	3.40	3.80	4.10	4.50	3.67
	h	2.00	10.00	11.00	8.00		31.00
PEN	V_s	2.60	3.00	3.95	4.15	4.50	3.66
	h	2.00	8.00	12.00	8.00		30.00
KCT	V_s	2.80	3.60	3.95	3.70	4.50	3.65
	h	2.00	11.00	6.00	10.00		29.00
YLV	V_s	2.80	3.20	3.90	4.10	4.60	3.68
	h	2.00	10.00	10.00	10.00		32.00
BOZ	V_s	3.20	3.60	3.20	3.80	4.70	3.52
	h	4.00	12.00	6.00	8.00		30.00
TAR	V_s	3.50	3.40	3.80	3.70	4.50	3.66
	h	3.50	7.00	12.50	12.00		35.00

thickness are perturbed and checked against the one standard deviation of the observed receiver functions. This analysis yields uncertainties of ±0.15 km s^{-1} in the crustal velocity and ±2 km in the crustal thickness.

8 CONCLUSIONS

The inversion results reveal that the velocity models for the stations installed on the same tectonic units are significantly similar to each other. Especially, the velocity models for the northern stations show only minor differences in their velocities and the Moho thicknesses. We observe crustal thinning from the south to north towards station TER. Nevertheless, the crustal thickness on the İstanbul–Zonguldak Zone is thickening from ∼30 km in west to 34 km beneath the easternmost station KLK. The thickest crustal estimate is beneath the southeast station TAR (35 km), located inland on the Sakarya Zone. (Fig. 8) The remarkably different velocity model for station BUY may be because of its proximity to the Çınarcık depression, although this station is on the same tectonic unit. However, the intermediate station YLV shows a velocity model that is very similar to the ones obtained for the northern stations. This can be interpreted as this station is being on the same tectonic unit as the northern stations (İstanbul–Zonguldak tectonic unit), since the Armutlu–Almacık Zone is thought to be a composite of the tectonic units of both the İstanbul–Zonguldak and the Sakarya Zones. The other intermediate station BOZ shows a quite different velocity model compared with the one obtained for station YLV. This station is located on a more complicated structure and is likely to have an LVZ by considering one standard deviation bound of its observed receiver function. LVZs were previously reported beneath the Basin and Range province (Landisman *et al.* 1971; Holbrook 1992; Özalaybey *et al.* 1997) and also beneath continental collision zones (Zor *et al.* 2003). The southern stations located on the Sakarya Zone show different velocity structure than the stations that are on the İstanbul–Zonguldak and Armutlu–Almacık Zones. Similarly, the easternmost station TAR in the Southern zone and station KLK in the Northern zone have close crustal thicknesses.

To sum up, we obtain that the average crustal thickness and *S*-wave velocity for the eastern Marmara region are 31 ± 2 km and 3.64 ± 0.15 km s^{-1}, respectively. The average crustal thickness we find is thicker than the crust (25 km) reported by Gürbüz & Üçer (1980), but much thinner than the results (39 km) obtained by Karahan *et al.* (2001). We do observe the crustal thickening from west (29–32 km) to east (34–35 km) along the NAFZ, but we observe no significant crustal thickness variation for the western part of the region from north to south while crossing the NAFZ. The average crustal thickness beneath continents is between 35 and 40 km with the exception of continental borderlands and island arcs and also thin crust occurs in continental borderlands and beneath the Basin and Range Province (Condie 1993). The eastern Marmara region with its important geothermal areas has high heat flow values changing between 40 and 180 mW m^{-2} (İlkişik 1995). The mean heat flow value for the region is 101 ± 11 mW m^{-2} and this is approximately 50 per cent higher than the world average. The region has also remarkable extensional features like the Çınarcık depression in the Marmara Sea. The Aegean region in the south with its uplifts, grabens and exhumations such as Menderes massive is thought to be a Basin and Range type extension. Combining all the information including our crustal thicknesses shows that the eastern Marmara region seems to have a Basin and Range type characteristic. However, the higher average crustal shear velocity (∼3.64 km s^{-1}) and the crustal thickening towards the east as evidenced by the southeasternmost station TAR (∼35 km) and KLK (∼34 km) indicate that the crust has also inland continental characteristics. Thus, we think that the eastern Marmara region is a transition zone between the extensional regime of Marmara Sea and the Aegean domain and continental Anatolian inland region.

ACKNOWLEDGMENTS

We thank Mustafa Aktar and Hayrullah Karabulut for their support. This work was supported in part by a project funded by Marmara Research Center of the Scientific and Technical Research Council of Turkey (TUBITAK).

REFERENCES

Ammon, C.J., Randall, R.E. & Zandt, G., 1993. On the nonuniqueness of Receiver function inversions, *J. geophys. Res.,* **95,** 15 303–15 318.

Barka, A., 1992. The North Anatolian Fault Zone, *Annales Tecton.,* **6,** 164–195.

Canıtez, N., 1962. Gravite anomalileri ve sismolojiye göre Kuzey Anadolu'da arz kabuğunun yapısı, *PhD thesis*, Istanbul Technical University, Istanbul.

Condie, C.K., 1993. *Plate Tectonics and Crustal Evolution*, Pergamon Press, New York.

Crampin, S. & Üçer, B., 1975. The seismicity of Marmara Sea region of Turkey, *Geophys. J. R. astr. Soc.,* **40,** 269–288.

Görür, N., Çağatay, M.N., Sakınç, M., Sümengen, K., Şenturk, K., Yaltirak, C. & Thapalyga, A., 1997. Origin of Sea of Marmara deduced from Neogene to Quaternary paleogeographic evolution of its frame, *Inter. Geol. Rev.,* **39,** 342–352.

Gürbüz, C., Üçer, B. & Özdemir, H., 1979. Adapazarı yöresinde yapılan yapay patlatma ile ilgili ön değerlendirme sonuçları, *Deprem Araştırma Bülteni (Turkey),* **31,** 73–88.

Gürbüz, C. & Üçer, B., 1980. Anadolu kavağında yapılan taş ocağı patlatmalarından elde edilen sismik kayıtların değerlendirilmesi, *Deprem Araştırma Bülteni (Turkey),* **49,** 39–49.

Holbrook, W.S., 1992. The crustal structure of the northwestern Basin and Range Province, Nevada, from Wide-Angle Seismic data, *J. geophys. Res.,* **95,** 21 843–21 869.

İlkişik, O.M., 1995. Regional heat flow in western Anatolia using silica temperature estimates from thermal springs, *Tectonophysics,* **244,** 175–184.

Karabulut, H.M., Bouin, M., Bouchon, M., Dietrich, C., Cornou, M. & Aktar, M., 2002. The seismicity in the eastern Marmara Sea after 17 August 1999 İzmit Earthquake, *Bull. seism. Soc. Am.,* **92,** 382–393.

Karabulut, H., Özalaybey, S., Taymaz, T., Aktar, M., Selvi, O. & Kocaoğlu, A., 2003. A tomographic image of the shallow crustal structure in the eastern Marmara, *Geophys. Res. Lett.,* **30,** doi: 10.1029/2003GL018074.

Karahan, A., Berckhemer, H. & Baier, B., 2001. Crustal structure at the western end of the North Anatolian Fault Zone from deep seismic sounding, *Annali di Geofisica,* **44,** 49–68.

Kenar, Ö., 1978. Sismik P dalgalarının genlik spectrumlarından yararlanarak Istanbul ve civarında yerkabuğu yapısı, *PhD thesis*, İ.T.Ü., Istanbul, Turkey.

Kennett, B.L.N., 1983. *Seismic wave propagation in stratified media*, Cambridge University Press, New York.

Kind, R. et al., 2002. Seismic Images of Crust and Upper Mantle Beneath Tibet: Evidence for Eurasia, *Science,* **298,** 1219–1221.

Landisman, M., Mueller, S. & Mitchell, B.J., 1971. Review of evidence for velocity inversions in the continental crust, *Am. Geophys. Union Mon.,* **14,** 11–34.

Langston, C., 1979. Structure under Mount Rainer Washington, Inferred from teleseismic body waves, *J. geophys. Res.,* **84,** 4749–4762.

Le Pichon, X. *et al.*, 2001. The active main Marmara fault, *Earth. planet. Sci. Lett.,* **192,** 595–616.

Liggoria, J.P. & Ammon, C.J., 1999. Iterative Deconvolution and receiver function estimation, *Bull. seism. Soc. Am.,* **89,** 1395–1400.

Necioğlu, A., Maddison, B. & Türkelli, N., 1981. A study of crustal and upper mantle structure of Northwestern Turkey, *Geophys. Res. Letts.,* **8,** 33–35.

Neidell, N.S. & Taner, M.T., 1971. Semblance and other coherency measures for multichannel data, *Geophysics,* **36**(3), 482–497.

Okay, A.I., Demirbağ, E., Kurt, H., Okay, N. & Kuşçu, I., 1999. An active, deep marine strike slip basin along the North Anatolian Fault in Turkey, *Tectonics,* **18,** 129–148.

Özalaybey, S., Savage, M.K., Sheehan, A.F., Louie, J.N. & Brune, J.N., 1997. Shear-wave velocity structure in the Northern Basin and Range Province from the combined analysis of receiver function and surface waves, *Bull. seism. Soc. Am.,* **87,** 183–199.

Özalaybey, S., Ergin, M., Aktar, M., Tapırdamaz, C., Biçmen, F. & Yörük, A., 2002. The 1999 Izmit Earthquake Sequence in Turkey: Seismological and Tectonic Aspects, *Bull. seism. Soc. Am.,* **92,** 376–386.

Rotstein, Y. & Kafka, A.L., 1982. Seismotectonics of southern boundary of Anatolia, eastern Mediterrenean region: subduction, collison and arc jumping, *J. geophys. Res.,* **87,** 7694–7706.

Sandvol, E., Şeber, D., Calvert, A. & Barazangi, M., 1998. Grid search modelling of receiver functions: Implications for crustal structure in the middle east and North Africa, *J. geophys. Res.,* **103,** 26 889–26 917.

Şengör, A.M.C., 1979. The North Anatolian Transform Fault: its age, offset and tectonic significance, *J. geol. Soc. Lond,* **136,** 269–282.

Şengör, A.M.C. & Yılmaz, Y., 1981. Tethyan evolution of Turkey: a plate tectonic approach: *Tectonophysics,* **75,** 181–241.

Tüysüz, O., Barka, A. & Yiğitbaş, E., 1998. Geology of Saros Graben: its implications on the evolution of the North Anatolian Fault in the Ganos-Saros region, NW Turkey, *Tectonophysics,* **293,** 105–126.

Yılmaz, Y., Tüysüz, O., Yigitbaş, E., Genç, S.C. & Şengör, A.M.C., 1997. Geology and Tectonic Evolution of the Pontides, in *Regional and petroleum geology of the Black Sea and surrounding region: AAPG Memoir 68*, pp. 183–226, ed. Robinson, A.G.

Zor, E., Sandvol, E., Gürbüz, C., Türkelli, N., Şeber, D. & Barazangi, M., 2003. The crustal structure of the East Anatolian Plateau (Turkey) from receiver functions, *J. geophys. Res.,* **30,** doi:10.1029/2003GL018192.